Methods for Computing Photogrammetric Refraction Corrections for Vertical and Oblique Photographs

Maurice S. Gyer

Abstract

Photogrammetric refraction computation methods for high oblique aerial photographs are derived from Snell's law for rays in a spherically stratified atmosphere. The methods, based on numerically integrating the refraction integrals, are applicable for zenith angles between 0 and 90 degrees. The atmospheric index of refraction is determined from atmospheric models of pressure and temperature. The models may be adjusted to reflect local pressure and temperature data when available. Standard aircraft pressurization procedures are used to evaluate the pressurized camera compartment refraction. Expressions are derived for the corrections to the image coordinates of photographs with arbitrary obliquity. The effects of different atmospheric models, geographic location, time of year, and large zenith angles are illustrated in the form of numerical tables and graphs. The results are applicable to determining the ground coordinates of points imaged with high oblique aerial surveillance cameras. A byproduct of the theory is a unified treatment of atmospheric refraction for arbitrary zenith angles.

Introduction

The methods developed by Barrow (1960), Faulds and Brock (1964), Bertram (1966), Bertram (1969), Forrest and Derouchie (1974), and Schut (1969) for computing photogrammetric refraction corrections become inadequate for zenith angles greater than 60°. A general approach, based on the rigorous refraction relationships for a ray in a spherically stratified model of the atmosphere permits computing the refraction for any zenith angle, including the case when the zenith angle equals 90° for some point on the ray. The resulting refraction integrals are expressed as functions of the atmospheric index of refraction. The index of refraction, as a function of altitude, is determined from averaged atmospheric models and local data if available. The atmospheric parameters are not incorporated directly in the refraction integrals (as in Bertram (1969), Saastamoinen (1972a), and Schut (1969)) to permit flexibility in the selection of present and future models and data. The results obtained complement those of Saastamoinen (1972a; 1972b; 1979) and reveal the regions of validity of various simplifying assumptions.

The results are applicable to determining the ground coordinates of points imaged with high oblique aerial surveillance cameras as illustrated in Figure 1. The positions and attitudes of the cameras for such missions are generally obtained by external positioning and attitude sensors (such as GPS and rate gyroscopes, respectively) without utilizing ground control points. Under such circumstances, refraction errors are not compensated by the elements of exterior orientation or general models of systematic errors in a bundle adjustment (e.g., Ebner, 1976), and precise refraction correction computations are required.

Spherically Stratified Model

Definitions of the symbols used in following sections are summarized in Table 1. The spherically stratified model of the atmospheric index of refraction is illustrated in Figure 2. The basic relationships are most easily expressed in polar coordinates with origin at the center of the model sphere and θ measured counterclockwise as illustrated. Snell's law for a spherically stratified model may be expressed as (Smart, 1977)

$$nr \sin \zeta = n_c r_c \sin \zeta_c = n_g r_g \sin \zeta_g = k = \text{constant}. \quad (1)$$

Letting $\theta = \theta(r)$, the equation of the ray path in polar coordinates is

$$\frac{rd\theta}{dr} = \tan \zeta \text{ or } d\theta = \frac{1}{r} \tan \zeta dr. \quad (2)$$

Equation 2 follows from the differential relationships illustrated in Figure 2 and may be found in elementary calculus textbooks. Integrating Equation 2 results in

$$\int_0^{\theta_c} d\theta = \theta_c = \int_{r_g}^{r_c} \tan \zeta \frac{1}{r} dr. \quad (3)$$

Another form of the refraction integral may be derived by differentiating Equation 1, i.e.,

$$dnr \sin \zeta + ndr \sin \zeta + nr \cos \zeta d\zeta = 0, \quad (4)$$

solving for dr

$$dr = -\frac{rdn}{n} - r \cot \zeta d\zeta, \quad (5)$$

substituting the result in Equation 2

$$d\theta + d\zeta = -\tan \zeta \frac{1}{n} dn, \quad (6)$$

and integrating

$$\int_{\theta_g}^{\theta_c} d\theta + \int_{\zeta_g}^{\zeta_c} d\zeta = \theta_c + \zeta_c - \zeta_g = -\int_{n_g}^{n_c} \tan \zeta \frac{1}{n} dn. \quad (7)$$

From triangle $P_c P_g O$ in Figure 3,

Eclectics, Inc., 103 Majesty Way, Port Angeles, WA 98362.

Photogrammetric Engineering & Remote Sensing, Vol. 62, No. 3, March 1996, pp. 301–310.

0099-1112/96/6203-301$3.00/0

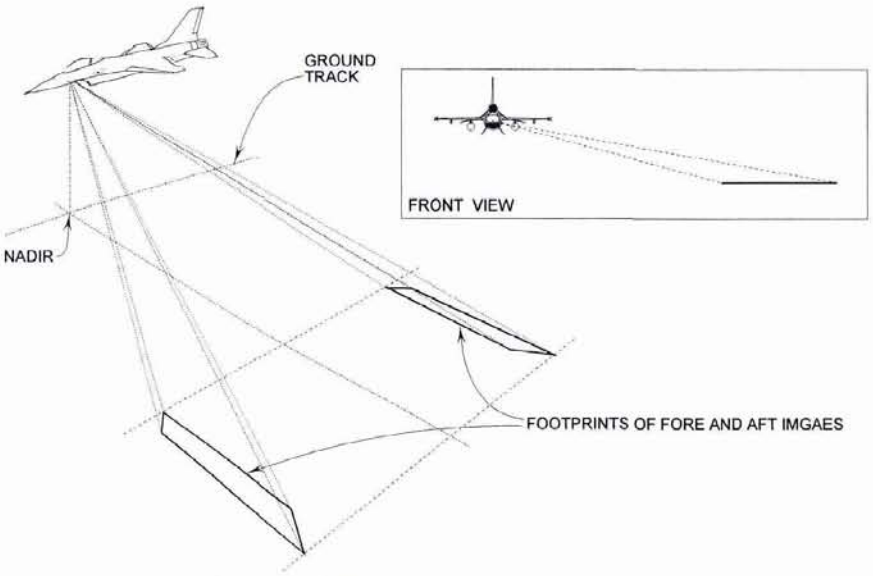

Figure 1. Oblique sidelooking fore and aft reconnaissance image acquisition.

$$\zeta_g + R_g = \theta_c + \zeta_c - R_c. \tag{8}$$

Substituting Equation 8 in Equation 7 results in

$$R_c + R_g = -\int_{n_g}^{n_c} \tan\zeta \frac{1}{n}\, dn. \tag{9}$$

Equations 3 and 9 are equivalent because given θ_c, $R_c + R_g$ may be obtained using Equations 1 and 8 and vice versa. Equation 9 is the form of the integral used to compute the astronomical refraction (Saastamoinen, 1979). In that case, the object may be assumed to be at infinity and $R_g = 0$. If the object is at a finite distance, $R_g \neq 0$ and θ_c must be determined, explicitly or implicitly, in order to determine R_c.

Evaluation of the Refraction Integral

The refraction angle (Figure 3) at the camera may be determined from

TABLE 1. DEFINITION OF SYMBOLS

Symbol	Definition
ζ_c,ζ,ζ_g	zenith angle of the refracted ray direction at the camera, at a point along ray, and at the ground point
n_c,n_g	atmospheric index of refraction (IOR) at the camera and ground point
n	IOR as function of altitude above sea level
r_e	radius of a sphere approximating curvature of ellipsoid
h_c,h,h_g	altitude of the camera, altitude of a point on ray path and elevation of a ground point, above sea level
r_g	$r_g = r_e + h_g$
r	$r = r_e + h$
r_c	$r_c = r_e + h_c$
θ	angle subtended at a center of a sphere by a ground point and a point on ray path
R_c,R_g	angle of refraction at the camera and a ground point
T,p	temperature and pressure as functions of altitude above sea level
e	partial vapor pressure
R_{cc}	pressurized camera compartment refraction
n_{cc},n_a	camera compartment and ambient IOR
ζ_a	camera field angle at the entrance to the camera window

$$\tan(\zeta_c - R_c) = \frac{\tan\zeta_c - \tan R_c}{1 + \tan\zeta_c \tan R_c} = \frac{r_g \sin\theta_c}{r_c - r_g\cos\theta_c} = \frac{\sin\theta_c}{r_c/r_g - \cos\theta_c}. \tag{10}$$

Solving for tan R_c results in

$$\tan R_c = \frac{\tan\zeta_c((r_c/r_g) - \cos\theta_c) - \sin\theta_c}{\tan\zeta_c \sin\theta_c + (r_c/r_g) - \cos\theta_c}. \tag{11}$$

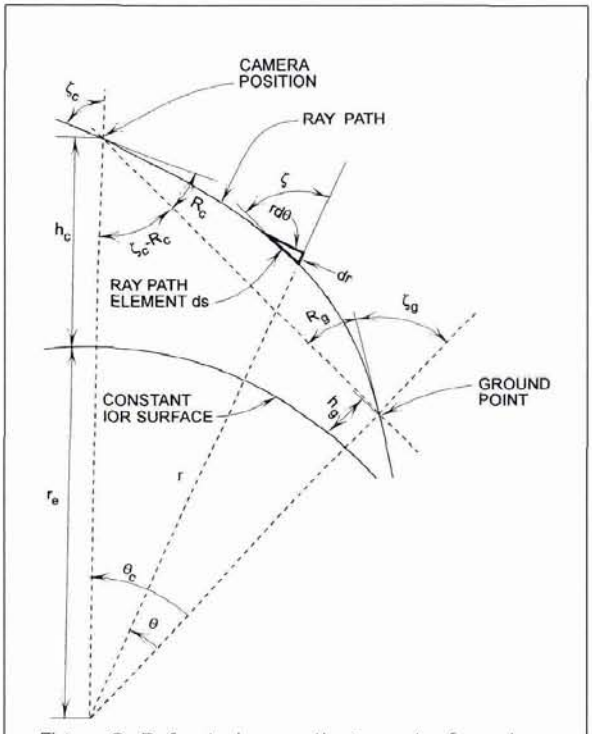

Figure 2. Refracted ray path geometry for spherically stratified atmosphere.

The explicit integral for θ_c is obtained by solving Equation 1 for sin ζ, substituting in tan ζ, substituting the result in Equation 3, and changing the variable of integration from r to h: i.e.,

$$\theta_c = \int_{r_g}^{r_c} \frac{1}{r} \tan\zeta dr = \int_{h_g}^{h_c} \frac{1}{r} \frac{\sin\zeta}{\cos\zeta} dr = \int_{h_g}^{h_c} \frac{k}{r\sqrt{n^2r^2 - k^2}} dr \quad (12)$$

where $dr = d(r_e + h) = dh$. The value for n may be computed from (Bomford, 1971, p. 50): i.e.,

$$n = 1 + 0.000078831 \frac{p}{T} - \frac{0.000011036e}{T}, \quad (13)$$

where T and p are expressed in degrees Kelvin (°K) and millibars, respectively. Pressure and temperature, as functions of h, may be obtained from atmospheric models modified by local observations, if available, as described below. The last term involving the partial vapor pressure in millibars, e, is negligible.

If $\zeta < 90°$ for all points on the ray path, the integrand in Equation 12 is a smooth monotonically decreasing function of h, and relatively simple numerical integration methods may be used to evaluate the integral. For certain values of ζ_c near 90°, ζ_g will equal 90° and the integral in Equation 12 will be improper because the denominator of the integrand will equal zero at the lower limit of integration. For large camera zenith distances, ζ may equal 90° for some point, P_{90}, (see Figure 4) on the ray path. Under this condition, the integrand is not montonically decreasing, the variable of integration is not monotonically increasing, and the elevations of two points on the ray path, P_g and P'_g (see Figure 4) are equal. If Equation 12 is evaluated using h_c and h_g as the limits of integration, the result will be θ'_c (see Figure 4), not θ_c. The integral must be evaluated as the sum of two improper integrals: i.e.,

$$\theta_c = \int_{h_{90}}^{h_c} I(h)dh + \int_{h_{90}}^{h_g} I(h)dh \quad (15)$$

where $I(h)$ is the integrand in Equation 12 and h_{90} is determined by iteratively solving

$$(r_e + h_{90})n(h_{90}) = r_c n_c \sin \zeta_c. \quad (16)$$

The existence of a P_{90} point on the ray path may not be obvious and an independent distance measurement may be required to resolve the ambiguity of whether P_g or P'_g (see Figure 4) is the correct point. The integration of the improper integrals is described below.

Plane Stratified Atmosphere

The methods in the previous section are derived from the rigorous refraction relationships for a spherically stratified atmospheric IOR model and may be applied to images acquired at any altitude and for any zenith angle. A plane stratified model of the index of refraction is adequate for vertical photography at aircraft altitudes and results in very simple formulas. The derivation may be expressed in cartesian coordinates using Snell's law (Figure 5) for a plane stratified model

$$n \sin \zeta = n_c \sin \zeta_c = n_g \sin \zeta_g \quad (17)$$

and the relationship between the derivative of the equation of the ray path and the zenith angle

$$\frac{dx}{dh} = \tan \zeta. \quad (18)$$

Solving Equation 17 for sin ζ, substituting the result in Equation 18, and factoring out cos ζ_c results in

$$\frac{dx}{dh} = \frac{n_c \sin \zeta_c}{\sqrt{n^2 - n_c^2 \sin^2 \zeta_c}} = \frac{n_c \sin \zeta_c}{\sqrt{n^2 - n_c^2 + n_c^2 \cos^2 \zeta_c}} = \frac{\tan \zeta_c}{\sqrt{1 + u}} \quad (19)$$

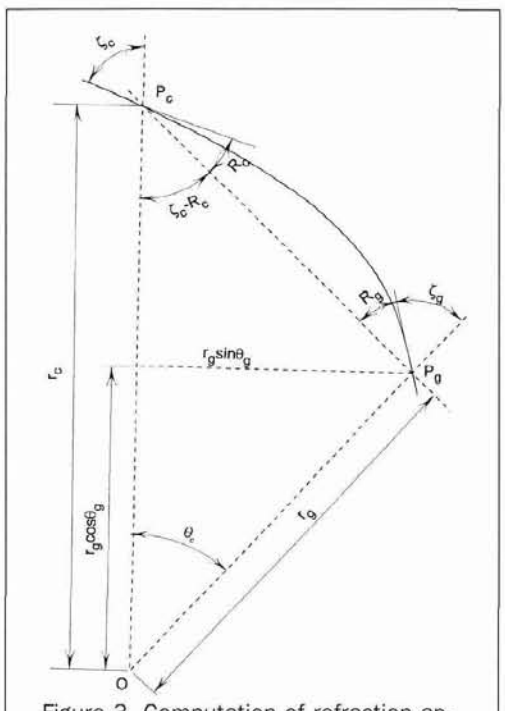

Figure 3. Computation of refraction angle.

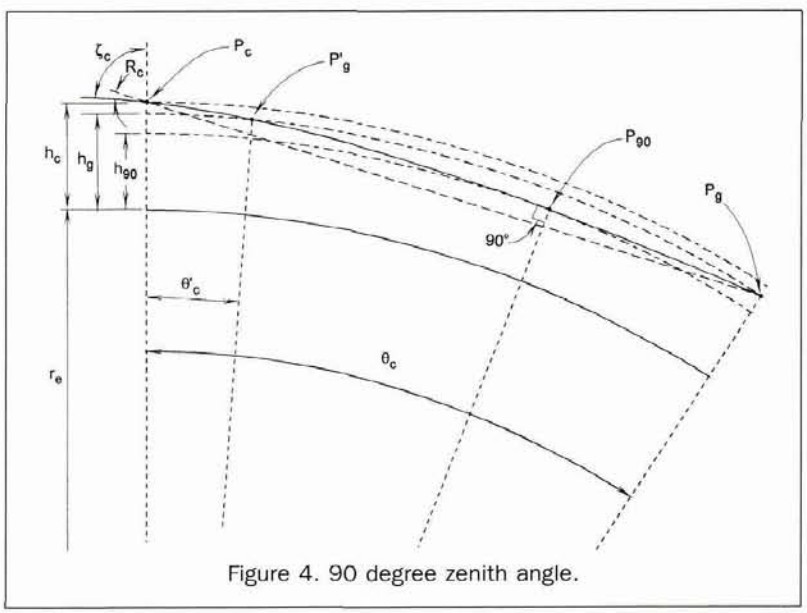

Figure 4. 90 degree zenith angle.

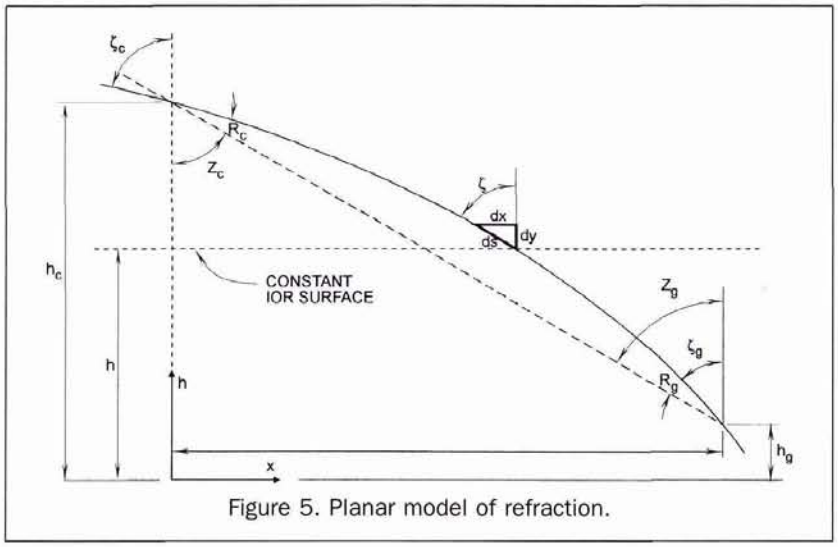

Figure 5. Planar model of refraction.

where

$$u = \frac{n^2 - n_c^2}{n_c^2 \cos^2 \zeta_c} = \frac{(n - n_c)(n + n_c)}{n_c^2 \cos^2 \zeta_c}.$$

Expressing the denominator of Equation 19 as a power series by the binomial theorem and integrating results in

$$x = \tan \zeta_c \int_{h_g}^{h_c} dh + \tan \zeta_c \int_{h_g}^{h_c} \left(-\frac{1}{2}u + \frac{3}{8}u^2 - \frac{5}{16}u^3 + \cdots\right) dh. \quad (20)$$

The first term may be approximated to the first order in R_c as follows:

$$\tan \zeta_c \int_{h_g}^{h_c} dh = (h_c - h_g)\tan(Z_c + R_c) \approx (h_c - h_g)\tan Z_c + \sec^2 Z_c (h_c - h_g)R_c = x + \sec^2 Z_c (h_c - h_g)R_c. \quad (21)$$

Substituting Equation 21 into Equation 20 results in the following explicit expression for the refraction at the camera:

$$R_c \approx \frac{\cos^2 Z_c \tan \zeta_c}{h_c - h_g} \int_{h_g}^{h_c} \left(\frac{1}{2}u - \frac{3}{8}u^2 + \frac{5}{16}u^3 - \cdots\right) dh. \quad (22)$$

Because R_c is small for zenith angles as large 60°, we may assume that

$$\frac{\cos^2 Z_c}{\cos^2 \zeta_c} \approx 1 \quad (23)$$

and express Equation 22 as

$$R_c \approx \frac{\tan \zeta_c}{h_c - h_g} \int_{h_g}^{h_c} \frac{1}{2} \frac{(n - n_c)(n + n_c)}{n_c^2} dh - \frac{\tan \zeta_c}{h_c - h_g} \int_{h_g}^{h_c} \left(\frac{3}{8}\left(\frac{(n - n_c)(n + n_c)}{n_c^2 \cos \zeta_c}\right)^2 + \frac{5}{16} \frac{(n - n_c)^3 (n + n_c)^3}{n_c^6 \cos^4 \zeta_c} - \cdots\right) dh \quad (24)$$

The first term in Equation 24 is essentially equivalent to Bertram's (1966; 1969) and Schut's (1969) results. The second and third terms are negligible for vertical photographs in the range of validity of the plane stratified model, i.e., $0 \le \zeta_c \le 60°$. The first term in Equation 24 may be easily evaluated by the numerical techniques described below.

Numerical Integration of the Refraction Integrals

The numerical integration of the refraction integrals consists of dividing the interval of integration into subintervals and approximating the integrand in a subinterval by a function that is easily integrated in terms of elementary functions. Thus, the refraction integrals may be expressed as

$$\Im = \sum_{i=1}^{i=n-1} \int_{h_i}^{h_{i+1}} I(h) dh \quad (25)$$

where

$h_1 = h_g$,
$h_{i+1} = h_i + \Delta h$,
Δh = step size,
$h_n = h_c$, and
$I(h)$ = the integrand in Equation 12 or Equation 24.

If we transform the variable of integration in each interval by

$$h' = \frac{1}{\Delta h}(h - h_i), \quad (26)$$

Equation 25 may be expressed as

$$\Im = \Delta h \sum_{i=1}^{i=n-1} \int_0^1 I(h') dh'. \quad (27)$$

Because $I(h) = I(h')$ is a smooth monotonically decreasing function, it may be approximated in the intervals $[h_i, h_{i+1}] = [h'_i, h'_{i+1}]$ by a third degree polynomial: i.e.,

$$I(h') \approx a_i + b_i h' + c_i h'^2 + d_i h'^3. \quad (28)$$

The polynomial coefficients in each interval are defined by $I(h'_{i-1})$, $I(h'_i)$, $I(h'_{i+1})$, and $I(h'_{i+2})$ where $h'_{i-1} = -1$, $h'_i = 0$, $h'_{i+1} = 1$, and $h'_{i+2} = 2$. The resulting coefficients are

$$\begin{aligned} a_i &= I(h_i) \\ b_i &= -\frac{1}{6}(2I(h_{i-1}) + 3I(h_i) - 6I(h_{i+1}) + I(h_{i+2})) \\ c_i &= \frac{1}{2}(I(h_{i-1}) - 2I(h_i) + I(h_{i+1})) \\ d_i &= -\frac{1}{6}(I(h_{i-1}) - 3I(h_i) + 3I(h_{i+1}) - I(h_{i+2})). \end{aligned} \quad (29)$$

The integrals in Equation 27 may be expressed in terms of the coefficients as

$$\int_{h_i}^{h_{i+1}} I(h)dh = \Delta h\left[\int_0^1 I(h')dh'\right] \approx \Delta h\left[a_i + \frac{1}{2}b_i + \frac{1}{3}c_i + \frac{1}{4}d_i\right]. \quad (30)$$

By substituting Equation 29 into Equation 30, the integrals may be expressed as

$$\int_{h_i}^{h_{i+1}} I(h)dh \approx \frac{\Delta h}{24}[-I(h_{i-1}) + 13I(h_i) + 13I(h_{i+1}) - I(h_{i+2})]. \quad (31)$$

Substituting Equation 31 into Equation 27 results in

$$\sum_{i=1}^{i=n-1}\int_{h_g}^{h_{i+1}} I(h)dh = \Delta h \sum_{i=3}^{i=n-2} I(h_i) + \Delta h\left[-\frac{1}{24}(I(h_0) + I(h_{n+1})) + \frac{1}{2}(I(h_1)+I(h_n)) + \frac{25}{24}(I(h_2)+I(h_{n-1}))\right] \quad (32)$$

where $h_0 = h_1 - \Delta h$ and $h_{n+1} = h_c + \Delta h$.

If ζ equals 90° at P_c, at P_g, or at a point on the ray path (Figure 4), the integrand in Equation 12 is singular. The integral may be evaluated by dividing the intervals containing and adjacent to P_{90} into small subintervals: i.e.,

$$\int_{h_k}^{h_\ell} \frac{kdh}{r\sqrt{n^2r^2 - k^2}} \approx \sum_{i=1}^{i=m-1}\int_{h_i}^{h_{i+1}} \frac{kdh}{r\sqrt{n_i^2r^2 - k^2}} = \sum_{i=1}^{i=m-1}\int_{h_i}^{h_{i+1}} \frac{(k/n_i)dh}{r\sqrt{r^2 - (k/n_i)^2}}, \quad (33)$$

where

$$h_i = h_k + (i-1)\frac{h\ell - h_k}{m-1}. \quad (34)$$

If we assume n is constant in each subinterval, the integrals may be expressed in terms of elementary functions: i.e.,

$$\int_{h_i}^{h_{i+1}} \frac{(k/n_i)dr}{r\sqrt{r^2-(k/n_i)^2}} = \cos^{-1}\left(\frac{k}{n_i r}\right)\Big|_{h_i}^{h_{i+1}} = \cos^{-1}\left(\frac{k}{n_i r_{i+1}}\right) - \cos^{-1}\left(\frac{k}{n_i r_i}\right). \quad (35)$$

The difference in evaluating Equation 15 by Equation 32 or Equation 35 for $\zeta_g < 90°$ are negligible when using small enough subintervals. This provides numerical evidence for the validity of the numerical integration procedures and the application of Equation 35 for the case where $\zeta_g = 90°$.

Pressurized Camera Compartment

The refraction of a ray entering a pressurized camera compartment is illustrated in Figure 6. If we assume that the window is an optical flat, the normals to the window surfaces are parallel and

$$n_{cc}\sin\zeta_f = n_c\sin\zeta_c = n_c\sin(\zeta_f - R_{cc}) \approx n_c\sin\zeta_f - n_c(\cos\zeta_f)R_{cc} \quad (36)$$

where the field angle, ζ_f, is given by

$$\zeta_f = \tan^{-1}\frac{\sqrt{x_m^2+y_m^2}}{f}. \quad (37)$$

Solving for R_{cc} results in

$$R_{cc} = -\tan\zeta_f\frac{n_{cc}-n_c}{n_c}. \quad (38)$$

Representative values of n_{cc} and R_{cc} for standard aircraft pressurization procedures (Ebeling, 1968) are given in Table 7.

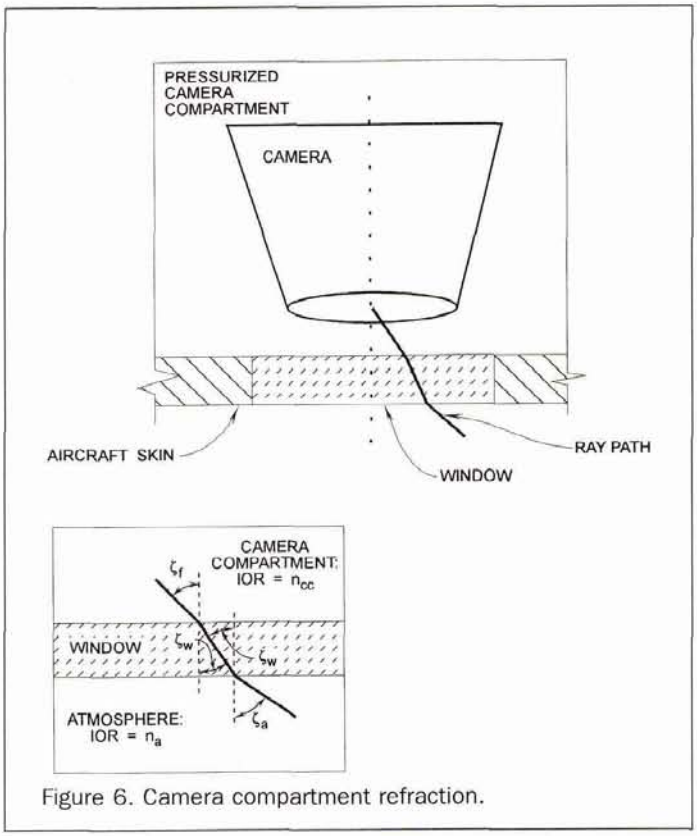

Figure 6. Camera compartment refraction.

The pressure difference between the compartment and the atmosphere may deform the window and result in some image distortion. A model of the effects of this distortion, assuming the deformed window is a spherical surface, is developed by Kushtin (1971a). Boundary layer effects are modeled by a thin prism by Andrade (1971) and a cylindrical surface by Kushtin (1971b). The effects of the boundary layer are apparently negligible at subsonic aircraft speeds or altitudes greater than 9,000 metres (Andrade, 1971).

Image Coordinate Corrections

In general, the corrections to the image coordinates for the effects of atmospheric refraction are radial with respect to the image of the camera nadir and the corrections for R_{cc} are radial with respect to the principal point (Figure 7). The nadir image and principal point are often assumed coincident for near vertical photography, and the corrections to the image coordinates due to R_c and R_{cc} may be combined as scalars. In general, for a photograph of arbitrary orientation (Faulds and Brock, 1964), the corrections must be combined as vectors (Figure 7).

n_{cc} is computed by Equation 13 using the best available data for the temperature and pressure in the camera compartment. The image coordinates corrected for R_{cc} are

$$x_{cc} = f\tan(\zeta_f + R_{cc})\frac{x_m}{\sqrt{x_m^2+y_m^2}} \approx x_m + \left(\frac{x_m}{x_m^2+y_m^2}f\sec^2\zeta_f\right)R_{cc} \text{ and}$$
$$y_{cc} = f\tan(\zeta_f + R_{cc})\frac{y_m}{\sqrt{x_m^2+y_m^2}} \approx y_m + \left(\frac{y_m}{\sqrt{x_m^2+y_m^2}}f\sec^2\zeta_f\right)R_{cc}, \quad (39)$$

where ζ_f is given by Equation 37. The coordinates of the nadir image are

$$x_n = -f\frac{C}{F} \text{ and}$$
$$y_n = -f\frac{C'}{F} \quad (40)$$

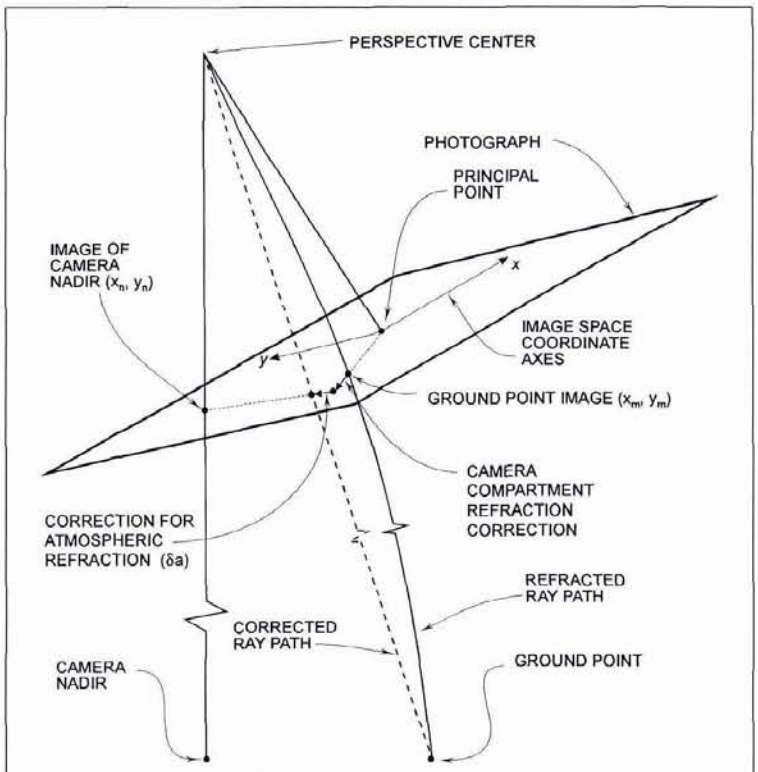

Figure 7. Correction to image coordinates.

where C, C', and F are entries of the orientation matrix, $\mathbf{M}$, of the photograph relative to the local vertical: i.e.,

$$\mathbf{M}=\begin{bmatrix} A & B & C \\ A' & B' & C' \\ D & E & F \end{bmatrix}. \tag{41}$$

See Wong (1980) for an exposition of frame camera geometry.

The apparent zenith angle may be computed by

$$\zeta_c=\cos^{-1}\left(\frac{f^2+x_n x_{cc}+y_n y_{cc}}{\sqrt{f^2+x_n^2+y_n^2}\ \sqrt{f^2+x_{cc}^2+y_{cc}^2}}\right). \tag{42}$$

Letting

$$a=\sqrt{(x_n-x_{cc})^2+(y_n-y_{cc})^2} \tag{43}$$

and

$$c=\sqrt{x_n^2+y_n^2+f^2}, \tag{44}$$

we have by the law of sines

$$a-\delta a=\frac{c\sin(\zeta_c-R_c)}{\sin(\beta+\zeta_c-R_c)} \tag{45}$$

where

$$\beta=\cos^{-1}\left(\frac{x_n(x_n-x_{cc})+y_n(y_n-y_{cc})}{\sqrt{x_n^2+y_n^2+f^2}\ \sqrt{(x_n-x_{cc})^2+(y_n-y_{cc})^2}}\right). \tag{46}$$

Solving Equation 44 for δR_c (Figure 6) results in

$$\delta a=a-\frac{c\sin(\zeta_c-R_c)}{\sin(\beta+\zeta_c-R_c)} \tag{47}$$

where R_c is computed by Equations 11 and 12 for a spherically stratified model or Equation 24 for a plane stratified model of the atmosphere. The integral in Equation 12 is evaluated numerically by Equation 32. A first-order expression in R_c for δa is given by

$$\delta a\approx a-\frac{c\sin\zeta_c}{\sin(\beta+\zeta_c)}+\left[\frac{c\cos\zeta_c}{\sin(\beta+\zeta_c)}-\frac{c\sin\zeta_c\cos(\beta+\zeta_c)}{\sin^2(\beta+\zeta_c)}\right]R_c. \tag{48}$$

Simplifying and combining terms results in

$$\delta a\approx a(\cot\zeta_c-\cot(\beta+\zeta_c))R_c. \tag{49}$$

The corrected image coordinates may now be expressed as

$$x_c = x_{cc}-\frac{x_n-x_{cc}}{a}\delta a \tag{50}$$

and

$$y_c=y_{cc}-\frac{y_n-y_{cc}}{a}\delta a, \tag{51}$$

where δa may be evaluated by Equation 47 or Equation 49.

Atmospheric Temperature and Pressure Models

A variety of atmospheric data and models for estimating T and p are available in the form of tables, computer code, and formulas. These include

- U.S. Standard Atmosphere developed by the Committee on Extension of the Standard Atmosphere (COESA, 1967; COESA, 1976);
- Air Force Geophysics Laboratory (AFGL) tables and models (Champion *et al.*, 1985; Cole and Kantor, 1978); and
- Marshall Space Flight Center (MSFC) computer programs and models (Johnson, 1990; Spiegler and Fowler, 1972).

The U.S. Standard Atmosphere and AFGL data are based on piecewise linear models of the variation of temperature with

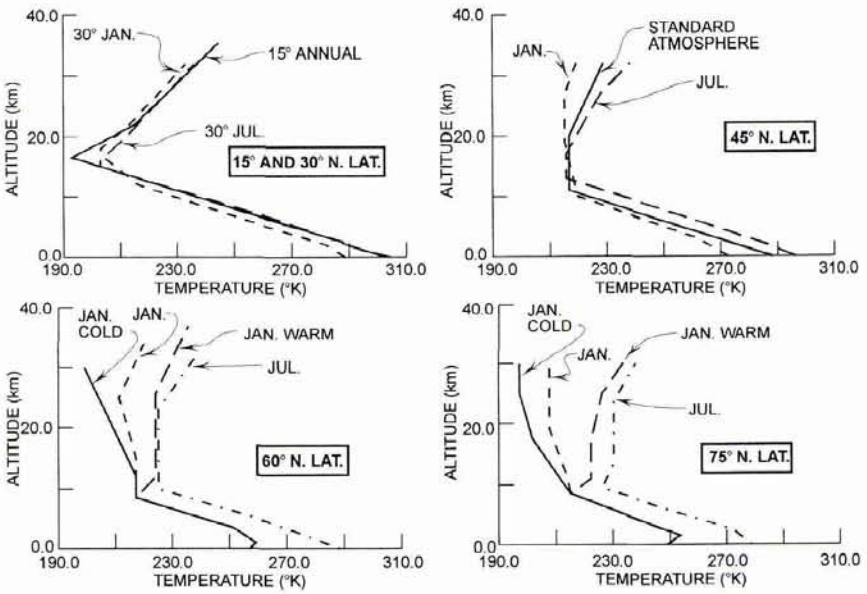

Figure 8. Temperature profiles: Standard and Extensions to Standard Atmosphere of 1966.

geopotential altitude, H. Pressure is computed from temperature profiles assuming the atmosphere is in hydrostatic equilibrium, is horizontally stratified, and the perfect gas law is applicable. The resulting formulas are (COESA, 1967, p. 12, Equation 33)

$$p=p_b\left(\frac{T_{Mb}}{T_{Mb}+L_b(H-H_b)}\right)^{\frac{g_\phi M_0}{R^* L_b}},\ L_b \neq 0 \qquad (52)$$

or

$$p=p_b\exp\left(-\frac{g_\phi M_0(H-H_b)}{R^* T_b}\right),\ L_b=0 \qquad (53)$$

where

L_b = the temperature gradient between the breakpoints of the temperature profile, b = 1, 2, 3 ...;
M_0 = molecular weight of air = 28.9644 kilograms/kilomole (kg/k-mol);
R^* = universal gas constant = 8.31432×10^3 joules/°K/k-mol;
T_b,p_b,H_b = the temperature, pressure, and geopotential altitude at the breakpoints of the temperature profile;
T_0,p_0 = temperature and pressure at sea level, H_0 = 0;
g_ϕ = acceleration of gravity (m/sec²) computed by

g_ϕ = $9.780356(1+0.0052885\sin^2\Phi - 0.0000059\sin^2 2\Phi)$;

Φ = geographic latitude;
H = geopotential altitude expressed in geopotential metres = $\frac{r_\phi h g_\phi}{(r_\phi + h)G}$;
h = geometric altitude;
r_ϕ = see List (1958), p. 218, Equation 6;
G = unit geopotential = 9.80665 m²/sec²;
m = geometric altitude (metres); and
m' = geopotential altitude (metres).

Thus, the tabular data in COESA (1967; 1976) may be com-

TABLE 2. ALTITUDE, PRESSURE, TEMPERATURE, AND IOR: STANDARD ATMOSPHERE 1976

Altitude (km)	Temperature (°K)	Pressure (mb)	IOR $(\mathbf{n}-1)\times10^{6}$*
−1	294.66	1139.30	304.80
0	288.16	1013.25	277.19
1	281.66	898.76	251.55
2	275.16	795.01	227.76
3	268.67	701.21	205.74
4	262.18	616.60	185.40
5	255.69	540.48	166.63
6	249.20	472.17	149.36
7	242.71	411.05	133.51
8	236.23	356.51	118.97
9	229.74	308.00	105.68
10	223.26	265.00	93.57
11	216.78	227.00	82.55
12	216.66	193.99	70.58
13	216.66	165.79	60.32
14	216.66	141.70	51.56
15	216.66	121.12	44.07
16	216.66	103.53	37.67
17	216.66	88.50	32.20
18	216.66	75.65	27.53
19	216.66	64.67	23.53
20	216.66	55.29	20.12
21	216.66	47.27	17.20
22	216.66	40.42	14.71
23	216.66	34.56	12.58
24	216.66	29.55	10.75
25	216.66	25.27	9.20
26	219.34	21.63	7.77

* index of refraction based on wavelength of light = 0.589 μm

TABLE 3. PHOTOGRAMMETRIC REFRACTION (ARC SEC): ζ_c = 45°, 60°, 75°

	ζ_c = 45°				ζ_c = 60°				ζ_c = 75°			
h_c (km)	h_g =0	h_g =2	h_g =4	h_g =6	h_g =0	h_g =2	h_g =4	h_g =6	h_g =0	h_g =2	h_g =4	h_g =6
1	2.61	—	—	—	4.52	—	—	—	9.76	—	—	—
2	4.97	—	—	—	8.61	—	—	—	18.58	—	—	—
3	7.09	2.24	—	—	12.28	3.88	—	—	26.53	8.37	—	—
4	8.98	4.25	—	—	15.57	7.37	—	—	33.65	15.91	—	—
5	10.67	6.05	1.91	—	18.49	10.49	3.31	—	40.00	22.66	7.13	—
6	12.15	7.65	3.61	—	21.07	13.26	6.26	—	45.62	28.67	13.51	—
7	13.46	9.06	5.13	1.61	23.33	15.71	8.89	2.79	50.57	33.99	19.19	6.02
8	14.59	10.30	6.47	3.04	25.30	17.86	11.21	5.27	54.88	38.67	24.22	11.38
9	15.56	11.37	7.64	4.31	26.98	19.72	13.24	7.46	58.60	42.75	28.64	16.12
10	16.38	12.30	8.65	5.41	28.41	21.33	15.00	9.38	61.78	46.27	32.49	20.28
11	17.06	13.08	9.53	6.38	29.61	22.69	16.53	11.06	64.45	49.29	35.83	23.92
12	18.01	14.12	10.66	7.58	31.26	24.50	18.48	13.14	68.11	53.26	40.10	28.45
13	18.67	14.86	11.47	8.46	32.40	25.79	19.90	14.67	70.67	56.12	43.22	31.80
14	19.08	15.36	12.04	9.10	33.13	26.65	20.89	15.78	72.35	58.08	45.44	34.24
15	19.31	15.67	12.43	9.55	33.53	27.20	21.56	16.56	73.33	59.34	46.95	35.98
16	19.39	15.82	12.66	9.85	33.68	27.48	21.97	17.09	73.75	60.04	47.90	37.17
17	19.35	15.86	12.77	10.03	33.62	27.55	22.18	17.41	73.74	60.30	48.42	37.93
18	19.22	15.81	12.79	10.12	33.40	27.47	22.22	17.57	73.38	60.21	48.58	38.33
19	19.01	15.69	12.74	10.14	33.06	27.26	22.13	17.60	72.76	59.85	48.47	38.46
20	18.76	15.50	12.63	10.10	32.62	26.95	21.95	17.54	71.92	59.28	48.15	38.37
21	18.46	15.28	12.48	10.01	32.11	26.57	21.69	17.39	70.93	58.54	47.66	38.11
22	18.13	15.02	12.29	9.88	31.55	26.13	21.36	17.18	69.83	57.68	47.03	37.72
23	17.78	14.74	12.07	9.73	30.94	25.65	21.00	16.92	68.63	56.73	46.31	37.22
24	17.41	14.44	11.84	9.56	30.32	25.14	20.60	16.63	67.38	55.72	45.52	36.64
25	17.03	14.14	11.59	9.37	29.68	24.62	20.18	16.31	66.10	54.66	44.68	36.00

puted from the appropriate piecewise linear temperature profiles (Figure 8), parameters, and constants. Additional details on the derivation and basis for the above formulas and extensive references may be found in COESA (1967; 1976), Champion *et al.* (1985), and Cole and Kantor (1978). If local observations and/or estimates of T and p are available, the COESA (1967; 1976) temperature profiles (Figure 8) may be modified, and improved pressure and IOR profiles may be computed using Equation 52, Equation 53, and Equation 13, respectively.

Numerical Results and Examples

Numerical results and examples based on the above theory are as follows:

- Representative values of n at 1-km intervals, based on the Standard Atmosphere 1976 (COESA, 1976), are given in Table 2;
- Representative values of R_c, based on (COESA, 1976) and a spherically stratified atmosphere, are given in Table 3 for ζ_c = 45°, 60°, and 75° and Table 4 for ζ_c = 80° and 85°;

TABLE 4. PHOTOGRAMMETRIC REFRACTION (ARC SEC): ζ_c = 80°, 85°

	ζ_c = 80°				ζ_c = 85°			
h_c (km)	h_g =0	h_g =2	h_g =4	h_g =6	h_g =0	h_g =2	h_g =4	h_g =6
1	14.84	0.00	0.00	0.00	30.12	0.00	0.00	0.00
2	28.30	0.00	0.00	0.00	57.84	0.00	0.00	0.00
3	40.47	12.74	0.00	0.00	83.35	25.85	0.00	0.00
4	51.41	24.24	0.00	0.00	106.77	49.55	0.00	0.00
5	61.20	34.56	10.85	0.00	128.26	71.23	22.02	0.00
6	69.91	43.80	20.59	0.00	147.97	91.05	42.10	0.00
7	77.61	52.01	29.28	9.16	166.04	109.13	60.38	18.60
8	84.38	59.27	37.02	17.34	182.63	125.64	77.01	35.48
9	90.27	65.64	43.84	24.60	197.86	140.67	92.07	50.75
10	95.34	71.17	49.82	31.00	211.89	154.37	105.73	64.53
11	99.67	75.95	55.03	36.62	224.88	166.90	118.11	76.98
12	105.51	82.21	61.67	43.61	241.38	182.77	133.68	92.46
13	109.71	86.78	66.58	48.82	255.23	195.74	146.16	104.65
14	112.57	90.01	70.14	52.67	267.06	206.47	156.24	114.37
15	114.38	92.18	72.64	55.46	277.50	215.54	164.53	122.21
16	115.36	93.50	74.30	57.43	287.08	223.46	171.48	128.64
17	115.67	94.17	75.29	58.74	296.29	230.63	177.47	133.98
18	115.47	94.31	75.76	59.53	305.62	237.41	182.81	138.54
19	114.86	94.03	75.81	59.89	315.57	244.19	187.79	142.54
20	113.93	93.43	75.53	59.92	326.77	251.31	192.68	146.21
21	112.77	92.59	75.00	59.69	340.01	259.22	197.75	149.75
22	111.42	91.56	74.27	59.26	356.47	268.41	203.27	153.34
23	109.95	90.39	73.39	58.67	378.14	279.62	209.61	157.19
24	108.39	89.12	72.40	57.95	409.18	293.96	217.20	161.53
25	106.77	87.78	71.33	57.15	465.69	313.44	226.69	166.64

TABLE 5. $R_c^{sph} - R_c^{pla}$ (ARC SEC), h_g = 0

h_c (km)	ζ_c = 45°	ζ_c = 60°	ζ_c = 75°	ζ_c = 80°	ζ_c = 85°
1	0.0	0.0	0.0	0.0	0.3
2	0.0	0.0	0.1	0.1	1.0
3	0.0	0.0	0.1	0.3	2.3
4	0.0	0.0	0.2	0.5	4.2
5	0.0	0.0	0.2	0.8	6.4
6	0.0	0.1	0.3	1.0	9.2
7	0.0	0.0	0.4	1.3	12.3
8	0.0	0.1	0.5	1.8	16.0
9	0.0	0.1	0.6	2.2	20.2
10	0.0	0.1	0.8	2.5	24.8
11	0.0	0.1	0.9	3.1	29.9
12	0.0	0.1	1.0	3.5	35.7
13	0.0	0.1	1.1	4.1	42.0
14	0.0	0.1	1.2	4.5	49.2
15	0.0	0.1	1.4	5.1	57.1
16	0.0	0.2	1.5	5.6	65.8
17	0.0	0.2	1.8	6.2	75.4
18	0.0	0.2	1.9	6.8	86.3
19	0.0	0.3	2.0	7.3	98.7
20	0.0	0.2	2.1	7.9	112.9
21	0.0	0.2	2.3	8.5	129.6
22	0.0	0.3	2.4	9.1	149.8
23	0.0	0.3	2.6	9.6	175.6
24	0.0	0.3	2.7	10.1	210.8
25	0.0	0.3	2.9	10.6	271.7

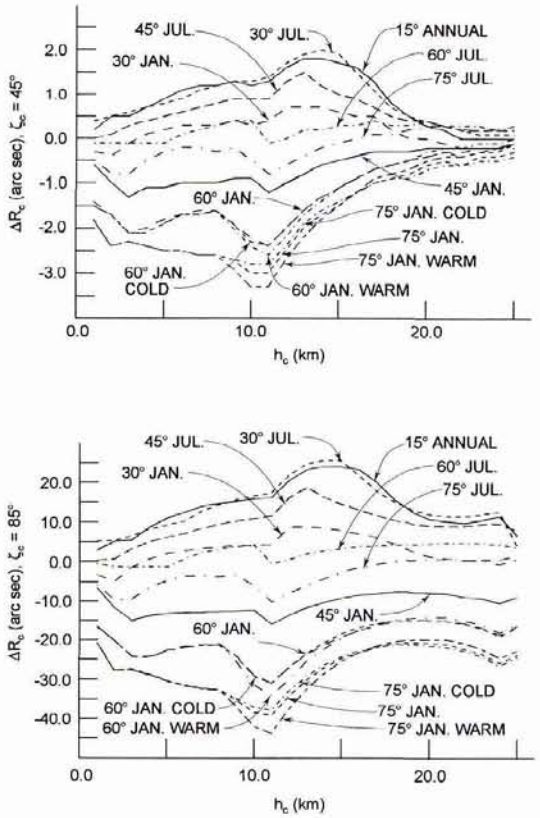

Figure 9. Differences in computed refraction: Standard Atmosphere - Extensions to Standard Atmosphere (h_g=0).

- Examples of $R_c^{sph} - R_c^{pla}$ are given in Table 5, where R_c^{sph} and R_c^{pla} are values of the refraction based on spherical and planar stratified atmospheric models, respectively;
- Examples of $\Delta R_c = R_c^{std} - R_c^{ext}$ are illustrated in Figure 9 for ζ_c = 45° and 85° and h_g = 0 where R_c^{std} and R_c^{ext} are the values of the refraction based on the Standard Atmosphere 1976 (COESA, 1976) and the Extensions to the Standard Atmosphere (COESA, 1967), respectively;
- Values of ζ_c and R_c for ζ_g = 90° and h_g = 0, illustrating the generality of the theory outlined above, are given in Table 6; and
- The effect of camera compartment pressurization (Table 7) was based on the following: (a) compartment temperature maintained at 70°F = 21.1°C; (b) compartment pressure equal to ambient pressure for $0 \le h_c \le 3$ km; and (c) compartment pressure maintained at 3 km pressure altitude (701.2 mb) for $3 < h_c \le 10$ km.

Summary

Our conclusions and recommendations, based on the above theory and numerical results, are as follows:

- Refraction computations based on the standard atmosphere (COESA, 1976) and a planar stratification model are adequate for near vertical wide angle and super wide angle photography (ζ_c <60°);
- If the camera compartment is pressurized, R_{cc} should be computed (using the best estimate of compartment temperature and pressure) and subtracted from the tabular or computed values of R_c;
- Refraction computations for oblique photographs, where ζ_c >60°, should be based on a spherical model of atmospheric stratification using the best temperature and pressure data available such as COESA (1967), Champion *et al.* (1985), Cole and Kantor (1978), or Johnson (1990);
- The atmospheric models, such as the COESA (1967) temperature profiles illustrated in Figure 8, may modified by local observations of temperature and pressure and a corrected pressure profile computed using Equations 52 and 53; and
- Corrections to the image coordinates of oblique photographs should be based on Equations 50 and 51.

TABLE 6. REFRACTION FOR ζ_g = 90°

	h_g = 0 km			h_g = 1 km			h_g = 2 km			h_g = 3 km		
h_c (km)	ζ_c (deg)	Dist. (km)	R_c (arc sec)	ζ_c (deg)	Dist. (km)	R_c (arc sec)	ζ_c (deg)	Dist. (km)	R_c (arc sec)	ζ_c (deg)	Dist. (km)	R_c (arc sec)
1	89.0721	123.	327.	—	—	—	—	—	—	—	—	—
2	88.6832	174.	445.	89.0656	123.	301.	—	—	—	—	—	—
3	88.3819	214.	525.	88.6743	173.	409.	89.0596	122.	277.	—	—	—
4	88.1257	246.	583.	88.3714	212.	482.	88.6660	172.	376.	89.0538	121.	254.
5	87.8980	275.	627.	88.1138	245.	536.	88.3614	211.	443.	88.6581	171.	345.
6	87.6907	301.	662.	87.8852	273.	576.	88.1027	243.	491.	88.3521	209.	406.
7	87.4986	325.	688.	87.6770	299.	607.	87.8731	271.	528.	88.0922	241.	450.
8	87.3188	347.	709.	87.4843	323.	631.	87.6642	297.	556.	87.8618	270.	483.
9	87.1489	368.	724.	87.3039	345.	649.	87.4709	321.	577.	87.6522	295.	508.
10	86.9873	387.	735.	87.1336	365.	662.	87.2900	342.	594.	87.4583	319.	527.
11	86.8328	405.	742.	86.9717	384.	672.	87.1193	363.	605.	87.2770	340.	542.
12	86.6865	423.	754.	86.8190	403.	686.	86.9592	382.	621.	87.1081	361.	560.
13	86.5449	440.	760.	86.6716	420.	693.	86.8054	401.	631.	86.9468	380.	571.
14	86.4075	456.	762.	86.5292	437.	696.	86.6572	418.	635.	86.7921	398.	577.
15	86.2740	472.	760.	86.3912	453.	696.	86.5141	435.	636.	86.6433	416.	580.
16	86.1443	487.	756.	86.2574	469.	693.	86.3758	451.	634.	86.4998	432.	579.
17	86.0181	501.	751.	86.1275	484.	688.	86.2418	466.	630.	86.3612	448.	576.
18	85.8951	515.	743.	86.0012	498.	682.	86.1117	481.	625.	86.2270	464.	571.
19	85.7753	529.	735.	85.8782	512.	675.	85.9854	495.	618.	86.0969	478.	565.
20	85.6583	543.	727.	85.7584	526.	667.	85.8624	509.	611.	85.9705	493.	559.
21	85.5441	555.	717.	85.6415	539.	658.	85.7427	523.	603.	85.8477	507.	552.
22	85.4324	568.	708.	85.5274	552.	649.	85.6259	536.	595.	85.7280	520.	544.
23	85.3232	580.	698.	85.4160	565.	641.	85.5120	549.	586.	85.6114	533.	537.
24	85.2163	592.	688.	85.3069	577.	631.	85.4007	562.	578.	85.4977	546.	528.
25	85.1116	604.	678.	85.2002	589.	622.	85.2918	574.	569.	85.3865	559.	521.

TABLE 7. PRESSURIZED CAMERA COMPARTMENT REFRACTION ($h_g = 0$, $\zeta_c = 45°$)

h_c (km)	$(n_c-1) \times 10^6$	$(n_{cc}-1) \times 10^6$	R_c (arc sec)	R_{cc} (arc sec)	$R_c - R_{cc}$ (arc sec)
1	251.54	240.77	2.61	−2.22	4.83
2	227.76	212.97	4.97	−3.05	8.02
3	205.74	187.84	7.09	−3.69	10.78
4	185.40	187.84	8.98	0.51	8.47
5	166.63	187.84	10.67	4.37	6.30
6	149.37	187.84	12.15	7.94	4.21
7	133.51	187.84	13.46	11.21	2.25
8	118.97	187.84	14.59	14.21	0.38
9	105.68	187.84	15.56	16.95	−1.39
10	93.57	187.84	16.38	19.44	−3.06

References

Andrade, J. B., 1977. *Photogrammetric Refraction,* PhD Thesis, The Ohio State University, Columbus, Ohio.

Barrow, Cran H., 1960. Very Accurate Correction of Aerial Photographs for the Effects of Atmospheric Refraction and Earth's Curvature, *Photogrammetric Engineering,* 26(5):798-804.

Bertram, S., 1966. Atmospheric Refraction, *Photogrammetric Engineering,* 32(1):76-84.

———, 1969. Atmospheric Refraction in Aerial Photogrammetry, *Photogrammetric Engineering,* 35(6):150.

Bomford, G., 1971. *Geodesy,* Clarendon Press, Oxford.

Champion, K.S.W., A.E. Cole, and K.J. Kantor, 1985. Standard and Reference Atmospheres, Chapter 14, *Handbook of Geophysics and the Space Environment* (A.E. Jursa, editor), Air Force Geophysics Laboratory, Hanscom Air Force Base, Bedford, Massachusetts, ADA 167000, National Technical Information Service, Springfield, Virginia.

COESA (Committee on Extension to the Standard Atmosphere), 1967. *U.S. Standard Atmosphere Supplements 1966,* U.S. Government Printing Office, Washington, D.C.

———, 1976. *U.S. Standard Atmosphere* 1976, National Oceanic and Atmospheric Administration, U.S. Government Printing Office, Washington, D.C.

Cole, A.E., and A.J. Kantor, 1978. *Air Force Reference Atmospheres,* AFGL TR 78-0051, Air Force Geophysics Laboratory, Hanscom Air Force Base, Bedford, Massachusetts, ADA 058505, National Technical Information Service, Springfield, Virginia.

Ebeling, A., 1968. *Fundamentals of Aircraft Environmental Control,* Hayden Book Co., New York.

Ebner, H., 1976. Self Calibrating Block Adjustment, *Archives, 13th Congress, International Society for Photogrammetry,* Helsinki, Finland, 11-13 July, Commission III, pp. 128-139.

Faulds, A.H., and R.H. Brock, 1964. Atmospheric Refraction and its Distortion of Aerial Photographs, *Photogrammetric Engineering,* 30(2):292-298.

Forrest, R.B., and W.F. Derouchie, 1974. Refraction Compensation, *Photogrammetric Engineering,* 40(5):577-582.

Johnson, D., 1990. *GRAM-90 Global Reference Atmospheric Model,* National Aeronautics and Space Administration, Marshall Space Flight Center, Huntsville, Alabama (program available through COSMIC, MFS 28577).

Kushtin, I.F., 1970. Photogrammetric Refraction of Light Rays with Allowance for Atmospheric Conditions Within the Aerial Camera Carrier, *Geodesy and Aerophotography,* (4):303-306.

———, 1971a. Internal Photogrammetric Refraction When There is Spherical Boundary Between the Air Layers, *Geodesy and Aerophotography,* (5):199-203.

———, 1971b. Refraction of Light in the Case of Separation of Gaseous Media by Lateral Surface of a Circular Cylinder, *Geodesy and Aerophotography,* (5):266-270.

List, R.J., 1958. *Smithsonian Meteorological Tables,* Smithsonian Institution, Washington, D.C.

Saastamoinen, J., 1972. Refraction, *Photogrammetric Engineering,* 38(8):799-810.

———, 1974. Local Variations in Photogrammetric Refraction, *Photogrammetric Engineering,* 40(3):295–301.

———, 1979. On the Calculation of Refraction In Model Atmospheres, *Refractional Influences in Astronometry and Geodesy* (E. Tengstrom, G. Teleki, and I. Ohlsson, editors), D. Reidel, Dordrecht and Boston.

Schut, G.H., 1969. Photogrammetric Refraction, *Photogrammetric Engineering,* 35(1):79-86.

Smart, W.M., and R.M. Green, 1977. *Textbook on Spherical Astronomy,* 6th Edition, revised, Cambridge University Press, Cambridge and New York.

Spiegler, D.B., and M.G. Fowler, 1972. *Four Dimensional World Wide Atmospheric Model to 25 Km Altitude,* N CR-2082, n 72-28638, National Aeronautics and Space Administration, Washington, D.C.

Wong, E.K., 1972. Basic Mathematics of Photogrammetry, *Manual of Photogrammetry,* 4th Edition (C.C Slama, editor), American Society for Photogrammetry, Falls Church, Virginia.

(Received 7 June 1993; revised and accepted 9 December 1994)